New Implicit Boundary Procedures—Theory and Applications

Man Mohan Rai*
Informatics General Corporation, Palo Alto, California

and

Denny S. Chaussee†
NASA Ames Research Center, Moffett Field, California

New implicit boundary procedures are presented for the Euler equations. These procedures use the theory of characteristics to update boundary points and are spatially second-order accurate. The boundary-point treatment presented is applicable to implicit schemes that employ approximate factorization, for example, the Beam-Warming scheme, and it differs from existing implicit inviscid boundary conditions in the following ways: 1) the boundary information is not used in a factored form, and 2) only one of the implicit inversion operators needs to be modified at the boundary. These differences result in a boundary procedure that is easy to incorporate in existing codes; they also result in small post-update corrections to the calculated boundary values. Demonstration calculations include flows over a cone and over a finned projectile. Significant increases in convergence rates are demonstrated for the conical flow solutions.

Introduction

THE increased use of implicit schemes for the solution of the Euler and Reynolds-averaged, Navier-Stokes equations has generated considerable interest in the development of stable, accurate, implicit boundary condition procedures. The application of viscous boundary conditions at the surface of a body in an implicit manner is a straightforward procedure. However, the application of accurate implicit boundary conditions for inviscid flows requires more detailed analysis. In the present paper, both the shock and body boundary conditions for inviscid flow are addressed.

In a recent paper, Chakravarthy[1] discussed in detail an approach based on the theory of characteristics to implement inviscid boundary conditions implicitly. The convergence rates were accelerated by an order of magnitude with the new boundary conditions (relative to explicit boundary conditions). The results in Ref. 1 are promising and warrant further investigation of implicit boundary procedures. The method discussed in this paper follows that of Ref. 1 very closely insofar as the theory of characteristics is used to update boundary points. However, the present method is different in two ways: 1) the method in which the approximate factorization is employed at the boundary, and 2) the manner in which the boundary information (surface tangency, Rankine-Hugoniot jump conditions, etc.) is included. It should be noted, however, that in one dimension the two methods are identical.

The main advantages of using the present approach are that the incorporation of boundary conditions is simple, and linear boundary conditions are satisfied identically. Thus, the magnitudes of post-update corrections to the boundary points in a nonlinear case can be expected to be small. A disadvantage of the present scheme is that adjacent boundaries cannot be treated using the characteristic approach. However, in many problems the boundaries that need to be updated using characteristics (i.e., the shock and body) are not adjacent but are opposite to each other and, hence, can be solved using the present method.

Submitted Nov. 29, 1982; presented as Paper 83-0123 at the AIAA 21st Aerospace Sciences Meeting, Reno, Nev., Jan. 10-13, 1983; revision submitted Aug. 4, 1983. This paper is declared a work of the U.S. Government and therefore is in the public domain.

*Principal Analyst. Member AIAA.
†Research Scientist. Member AIAA.

This paper also discusses some of the details that need to be addressed in the case of moving boundaries; for example, shocks. The number of unknowns at a moving boundary is greater than the number of dependent variables. The additional unknowns result from the motion of the boundary. The correct treatment of all the unknowns is crucial in obtaining time-accurate results.

The current implicit boundary procedure has been incorporated into an existing parabolized Navier-Stokes (PNS) code.[2] Substantial decreases in convergence times for the calculation of conical flowfields are demonstrated. The paper also includes results obtained with the new PNS code for supersonic viscous flow over a finned projectile.

Boundary Procedure

To describe the procedure, consider the unsteady Euler equations in two dimensions,

$$Q_t + E_x + F_y = 0 \tag{1}$$

where

$$Q = \begin{bmatrix} \rho \\ \rho u \\ \rho v \\ e \end{bmatrix} \quad E = \begin{bmatrix} \rho u \\ p + \rho u^2 \\ \rho uv \\ (e+p)u \end{bmatrix} \quad F = \begin{bmatrix} \rho v \\ \rho uv \\ p + \rho v^2 \\ (e+p)v \end{bmatrix} \tag{2}$$

and ρ is the density; p the pressure; u and v the velocities in the x and y directions, respectively; and e the total energy per unit volume. Applying the independent-variable transformation

$$\tau = t, \qquad \xi = \xi(x, y, t), \qquad \eta = \eta(x, y, t) \tag{3}$$

to Eq. (1) yields

$$\tilde{Q}_\tau + \tilde{E}_\xi + \tilde{F}_\eta = 0 \tag{4}$$

where

$$\begin{aligned} \tilde{Q} &= Q/J \\ \tilde{E} &= \left[\xi_t Q + \xi_x E + \xi_y F\right]/J \\ \tilde{F} &= \left[\eta_t Q + \eta_x E + \eta_y F\right]/J \\ J &= \xi_x \eta_y - \eta_x \xi_y \end{aligned} \tag{5}$$

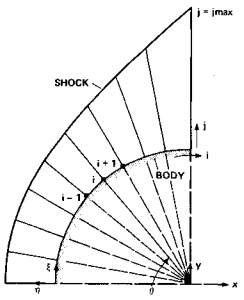

Fig. 1 Physical domain for the cylinder in a supersonic freestream.

Let the Jacobian matrices $\tilde{A}$ and $\tilde{B}$ be defined as

$$\tilde{A}=\frac{\partial \tilde{E}}{\partial \tilde{Q}}, \qquad \tilde{B}=\frac{\partial \tilde{F}}{\partial \tilde{Q}} \tag{6}$$

Consider a constant η boundary surface such that the region of interest lies above this boundary (e.g., the body surface in Fig. 1). At any point along this boundary only forward differences, i.e., into the flowfield, are available in the η direction. Both backward and forward differences are possible in the ξ direction. Hence, the ξ derivatives in Eq. (4) can be approximated easily using conventional central differences. Let L be the matrix of left eigenvectors of $\tilde{B}$,

$$L=\begin{bmatrix} e_1 \\ e_2 \\ e_3 \\ e_4 \end{bmatrix} \tag{7}$$

The necessary form of the compatibility equations is obtained by multiplying Eq. (4) by e_1, e_2, etc., and, in a compact form, can be written as

$$L\left(\tilde{Q}_\tau+\tilde{E}_\xi+\tilde{F}_\eta\right)=0 \tag{8}$$

Details regarding the derivation of the compatibility equations and the matrix L are given in Refs. 1 and 3. The finite difference form of Eq. (8), using the Beam-Warming linearization,[4] is given by

$$L^n\left[I+\Delta\tau\delta_\xi\tilde{A}^n+\Delta\tau\delta_\eta\tilde{B}^n\right]\Delta\tilde{Q}=-\Delta\tau L^n\left[\delta_\xi\tilde{E}^n+\delta_\eta\tilde{F}^n\right] \tag{9}$$

where n is the index in the τ direction. The implicit and explicit smoothing terms have been left out of Eq. (9) for the sake of simplicity. The derivations that follow remain unchanged except for the addition of the smoothing terms.

Some of the eigenvectors in L correspond to positive eigenvalues of $\tilde{B}$, and, since these eigenvectors represent information coming into the region of interest from the boundary, the corresponding compatibility equations are not valid at the boundary in question. Denote L_2 as

$$L_2=\begin{bmatrix} e_1 \\ \vdots \\ e_p \\ 0 \\ \vdots \\ 0 \end{bmatrix} \tag{10}$$

where $e_1 \cdots e_p$ are the eigenvectors that correspond to the negative eigenvalues of $\tilde{B}$. Let the boundary conditions be given by

$$B_i(\tilde{Q})=0 \qquad i=p+1,\ldots,4 \tag{11}$$

Equation (11) may represent surface tangency or the Rankine-Hugoniot jump conditions for example. Linearizing Eq. (11) with respect to $\tilde{Q}$, the following is obtained:

$$\frac{\partial B_i}{\partial \tilde{Q}}\Delta\tilde{Q}\simeq 0 \tag{12}$$

To illustrate the linearization process, consider the Rankine-Hugoniot (R-H) jump conditions, which are applied across a shock, and for the region in Fig. 1 are given by

$$\eta_t(Q-Q_\infty)+\eta_x(E-E_\infty)+\eta_y(F-F_\infty)=0 \tag{13}$$

where the subscript ∞ indicates conditions on the freestream side of the shock. Equation (13) is a vector equation comprising four scalar equations. Assuming that the metrics of the transformation are constant over the integration step (except for η_t, which is a measure of the shock speed), Eq. (13) can be linearized as

$$(Q-Q_\infty)^n\Delta\eta_t+\left(\eta_t I+\eta_x\frac{\partial E}{\partial Q}+\eta_y\frac{\partial F}{\partial Q}\right)\Delta Q=0 \tag{14}$$

or

$$(\tilde{Q}-\tilde{Q}_\infty)^n\Delta\eta_t+\tilde{B}^n\Delta\tilde{Q}=0 \tag{15}$$

Equation (15) is a system of four equations with five unknowns ($\Delta\eta_t$ and $\Delta\tilde{Q}$) and can be reduced to a system of three equations and four unknowns ($\Delta\tilde{Q}$ alone) by simple algebraic manipulation. The unknown $\Delta\eta_t$ is removed from Eq. (15) in order that the linearized R-H equations can be incorporated into Eq. (9). The removal of the unknown $\Delta\eta_t$ from Eq. (15) will result in a system of equations of the form given in Eq. (12). Let L_1 be given by

$$L_1=L_2+\begin{bmatrix} 0 \\ \vdots \\ 0 \\ \dfrac{\partial B_{p+1}}{\partial \tilde{Q}} \\ \vdots \\ \dfrac{\partial B_4}{\partial \tilde{Q}} \end{bmatrix} \tag{16}$$

The compatibility equations, which are not valid at the boundary, must be replaced with the pertinent boundary information. To do this, L is replaced with L_1 and L_2 in Eq. (9) in the following manner:

$$\left[L_1^n+\Delta\tau L_2^n\delta_\xi\tilde{A}^n+\Delta\tau L_2^n\delta_\eta\tilde{B}^n\right]\Delta\tilde{Q}=-\Delta\tau L_2^n\left[\delta_\xi\tilde{E}^n+\delta_\eta\tilde{F}^n\right] \tag{17}$$

yielding the appropriate system of equations to be solved at the boundary. Note that Eq. (17) is merely a combination of Eq. (12) and the appropriate compatibility equations of Eq. (9). Equation (17) is not in a factored form and is, hence, extremely time consuming to solve.

To overcome this problem, the approach taken in Ref. 1 was to multiply Eq. (17) by L_1^{-1} and factor the left-hand side of the resulting equation to yield

$$\left(I+\Delta\tau(L_1^n)^{-1}L_2^n\delta_\xi\tilde{A}^n\right)\left(I+\Delta\tau(L_1^n)^{-1}L_2^n\delta_\eta\tilde{B}^n\right)\Delta\tilde{Q}$$
$$=-\Delta\tau(L_1^n)^{-1}L_2^n\left(\delta_\xi\tilde{E}^n+\delta_\eta\tilde{F}^n\right) \tag{18}$$

In contrast, the boundary conditions that are developed in this study take the final form of

$$\left(L_1^n + \Delta\tau L_2^n \delta_\eta \tilde{B}^n\right)\Delta\tilde{Q} = -\Delta\tau L_2^n \left(I + \Delta\tau \delta_\xi \tilde{A}^n\right)^{-1}\left(\delta_\xi \tilde{E}^n + \delta_\eta \tilde{F}^n\right) \tag{19}$$

Equation (19) is obtained by taking the factored form of the Euler equations (i.e., before they are multiplied by L), carrying out the first inversion, and then multiplying these resulting equations by the appropriate eigenvectors. The linearized boundary information is then included to yield Eq. (19). The terms $\delta_\eta \tilde{B}^n$ and $\delta_\eta \tilde{F}^n$ in Eq. (19) are evaluated using either three-point backward or forward differences, depending on whether the boundary is an upper or lower boundary. This differencing maintains second-order accuracy in the spatial direction. The use of the three-point, one-sided difference in evaluating $\delta_\eta \tilde{B}^n$ destroys the block-tridiagonal nature of the matrices involved. However, this desirable block-tridiagonal property is restored by using simple algebraic manipulation.

Equation (19) is not strictly characteristic in nature in the sense of Eq. (17), because the multiplication by the eigenvectors is carried out after the first inversion. The error that is introduced by using Eq. (19) instead of Eq. (17) can be shown to be of the same order as the truncation error of the first-order-accurate Beam-Warming scheme (i.e., in the marching direction). This allows the more convenient form of the equations to be used at the boundaries without degrading the accuracy of the solution. The details of this proof are given in Ref. 5.

Since the first inversion in Eq. (19), $(I + \Delta\tau\delta_\xi \tilde{A}^n)^{-1}(\delta_\xi \tilde{E}^n + \delta_\eta \tilde{F}^n)$, is performed without any regard to the fact that the point in question is a boundary point, the present method can be implemented in existing Euler, Navier-Stokes, and PNS codes with minor modifications to these codes. In contrast, the boundary procedure used in Ref. 1 requires the calculation of modified inversion operators in both the ξ and η directions, instead of in the η direction alone. Also, since the boundary information is incorporated after the first inversion, this information will not be contaminated by the approximate factorization error. As a result, linear boundary conditions will be satisfied exactly, and the post-update corrections to the boundary points in a nonlinear case can be expected to be small in magnitude. In fact, it was found that post-update corrections were not required for the cases that have been calculated so far.

In order to obtain accurate results at large Courant numbers, with the implicit boundary conditions described above, it is important to treat the metrics of the transformation implicitly. To illustrate this aspect of the boundary procedure we consider the two-dimensional problem of a cylinder in a supersonic freestream with the associated detached bow shock (see Fig. 1). The bow shock is used as a boundary of the computational plane, and the grid is generated by drawing straight-line rays from the center of the cylinder and placing points equidistantly along each ray. The Rankine-Hugoniot jump conditions are given by Eq. (13). For this problem it has been shown that only the compatibility equation corresponding to the positive eigenvalue

$$\lambda = \eta_t + u\eta_x + v\eta_y + c\left(\eta_x^2 + \eta_y^2\right)^{\frac{1}{2}}$$

is valid at the shock. Since the shock is moving, the metrics are also unknown at the new time level; hence, six new unknowns are introduced. They are $x_\tau, y_\tau, x_\xi, y_\xi, x_\eta, y_\eta$. Since the R-H conditions and the compatibility equation together only furnish a total of five equations, five additional equations are required to solve for the 10 unknowns (4 flow and 6 geometric). These additional equations are obtained from geometric considerations.

Assuming that the shock moves along the fixed rays, it can be shown that

$$x_{\tau_{i,j\max}}^{n+1}\sin\theta + y_{\tau_{i,j\max}}^{n+1}\cos\theta = 0 \tag{20}$$

and, assuming the grid is regenerated so that the points are always placed equidistantly along the rays, it is possible to write

$$x_{\eta_{i,j\max}}^{n+1} = x_{\eta_{i,j\max}}^{n} + \Delta\tau x_{\eta\tau_{i,j\max}}^{n+1} = x_{\eta_{i,j\max}}^{n} + \left[\Delta\tau x_{\tau_{i,j\max}}^{n+1}\right]/[j\max - 1] \tag{21}$$

where i and j are the indices in the ξ and η directions, respectively, and $j\max$ is the number of points in the η direction. The calculation of $x_{\xi_{i,j\max}}^{n+1}$ and $y_{\xi_{i,j\max}}^{n+1}$ is not quite as simple, because if we were to write

$$x_{\xi_{i,j\max}}^{n+1} = x_{\xi_{i,j\max}}^{n} + \Delta\tau x_{\xi\tau_{i,j\max}}^{n+1} = x_{\xi_{i,j\max}}^{n} + \Delta\tau\left[x_{\tau_{i+1,j\max}}^{n+1} - x_{\tau_{i-1,j\max}}^{n+1}\right]/2 \tag{22}$$

(using a conventional central difference to calculate the ξ derivatives), there would be a coupling in the ξ direction that would not allow the use of the factored form of the governing differential equations. However, as a first approximation, x_τ^{n+1} can be replaced by x_τ^n in Eq. (22). Expressions similar to Eqs. (21) and (22) can be obtained for y_η^{n+1} and y_ξ^{n+1}, thus resulting in a total of five geometric constraints.

Similar considerations apply at a body surface except that the calculation of x_ξ^{n+1} and y_ξ^{n+1} is trivial since they do not vary in time (stationary body). Equations (21) and (22) supply the required amount of information to make the problem determinate.

If only the time-asymptotic solution is required, the values of the metrics can be set to their values at time level n with no loss in accuracy. Thus, the above procedure for calculating the metrics used in the R-H conditions and the relevant compatibility equations is required only for solutions that need to be accurate in the marching direction. Equation (21) was obtained by making the assumption that the grid is regenerated so that the points are always placed equidistantly along the straight-line rays. In the general case, when the grid lines are curved and the points are not equidistant, the information pertaining to how the grid is regenerated will have to be incorporated in the boundary procedure.

Extension to Three Spatial Dimensions

In three spatial dimensions the unsteady Euler equations are given by

$$\tilde{Q}_\tau + \tilde{E}_\xi + \tilde{F}_\eta + \tilde{G}_\zeta = 0 \tag{23}$$

where

$$\tilde{Q} = Q/J$$
$$\tilde{E} = \left[\xi_t Q + \xi_x E + \xi_y F + \xi_z G\right]/J$$
$$\tilde{F} = \left[\eta_t Q + \eta_x E + \eta_y F + \eta_z G\right]/J$$
$$\tilde{G} = \left[\zeta_t Q + \zeta_x E + \zeta_y F + \zeta_z G\right]/J$$
$$J = \xi_x\left(\eta_y\zeta_z - \eta_z\zeta_y\right) + \xi_y\left(\eta_z\zeta_x - \eta_x\zeta_z\right) + \xi_z\left(\eta_y\zeta_x - \eta_x\zeta_y\right) \tag{24}$$

and

$$Q=\begin{bmatrix}\rho\\ \rho u\\ \rho v\\ \rho w\\ e\end{bmatrix} \qquad E=\begin{bmatrix}\rho u\\ p+\rho u^2\\ \rho uv\\ \rho uw\\ (e+p)u\end{bmatrix}$$

$$F=\begin{bmatrix}\rho v\\ \rho uv\\ p+\rho v^2\\ \rho vw\\ (e+p)v\end{bmatrix} \qquad G=\begin{bmatrix}\rho w\\ \rho uw\\ \rho vw\\ p+\rho w^2\\ (e+p)w\end{bmatrix} \tag{25}$$

Proceeding as before we obtain the boundary equations

$$\left[L_1^n+\Delta\tau L_2^n\delta_\zeta\tilde{C}^n\right]\Delta\tilde{Q}=-\Delta\tau L_2^n\left[I+\Delta\tau\delta_\eta\tilde{B}^n\right]^{-1}$$
$$\times\left[I+\Delta\tau\delta_\xi\tilde{A}^n\right]^{-1}\left[\delta_\xi\tilde{E}^n+\delta_\eta\tilde{F}^n+\delta_\zeta\tilde{G}^n\right] \tag{26}$$

where $\tilde{A}$, $\tilde{B}$, and $\tilde{C}$ are the Jacobian matrices and L_1 and L_2 are defined in a manner similar to that in Eqs. (10) and (16), with L as the matrix of left eigenvectors of $\tilde{C}$. It is assumed that the boundaries are constant ζ surfaces.

The three-dimensional steady Euler equations are given by

$$\tilde{E}_\xi+\tilde{F}_\eta+\tilde{G}_\zeta=0 \tag{27}$$

For streamwise space-marching procedures such as the PNS code, the equation corresponding to Eq. (26) takes the form

$$\left[L_1^n+\Delta\xi L_2^n(\tilde{A}^n)^{-1}\delta_\zeta\tilde{C}^n\right]\Delta\tilde{Q}$$
$$=-\Delta\xi L_2^n\left[\tilde{A}^n+\Delta\xi\delta_\eta\tilde{B}^n\right]^{-1}\left[\delta_\eta\tilde{F}^n+\delta_\zeta\tilde{G}^n\right] \tag{28}$$

where $\tilde{A}$, $\tilde{B}$, and $\tilde{C}$ are the Jacobian matrices, n is the index in the ξ or marching direction, and L_1 and L_2 are defined as in Eqs. (10) and (16) but with L as the matrix of left eigenvectors of $\tilde{A}^{-1}\tilde{C}$. It can be shown that the error introduced by using Eqs. (26) and (28) instead of the unfactored forms of these equations [corresponding to Eq. (17)] is of the same magnitude as the truncation error of the integration scheme. The proof is similar to the one given in Ref. 5.

Results

The implicit boundary procedures described above [Eq. (28)] have been incorporated into a current PNS code at the shock and body surfaces. This gives the code the additional capability to operate implicitly in either the viscous or inviscid mode. In the inviscid mode, both the body and the shock are treated using the implicit scheme developed in this paper. In the viscous mode, only the shock is treated with the present scheme (the shock is assumed to lie in the inviscid region). The dependent variables at the body are updated using a standard implicit viscous boundary condition.[6] The code also has the additional option of using cylindrical or Cartesian base coordinate systems as frames of reference for calculations. Conical solutions are obtained by using the code in a step-back mode where the solution is marched forward through one spatial step and then stepped back by making use of the conical flow assumption.[7] The remainder of this section presents results that exercise these new options.

Conical Flows

To test the new implicit shock-fitting and body-surface routines, a simple supersonic cone flow was chosen. It consisted of a $M_\infty=4$ inviscid flow past a 5-deg cone at 0-deg angle of attack. Three points in the circumferential direction and 23 equispaced points in the radial direction were used for the calculation, together with the cylindrical coordinate system option. (The cylindrical coordinate system option requires the use of only three points in the circumferential direction for axisymmetric cases, whereas the Cartesian formulation requires a minimum of 19 points to resolve the metrics correctly.) The advantage in using the new implicit shock and body boundary conditions is evident from Fig. 2, in which iterations to convergence vs Courant number ν are presented. The method with explicit boundary conditions was stable only for Courant numbers less than 0.7 and needs approximately 525 steps for convergence at this value of ν. At a Courant number of 62.6 only 11 steps were required for convergence. The use of the implicit boundary conditions resulted in the solution converging 48 times faster. The error in the surface density was less than 0.5% at all values of ν. For this case it was not possible to use values of ν larger than 62.6, because the step size was so large that the first plane of data (required for the step-back procedure) fell upstream of the cone. This problem does not occur in time-dependent calculations.

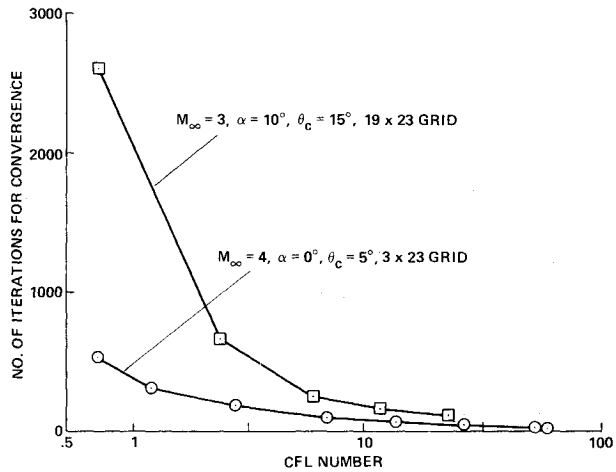

Fig. 2 Convergence rate for inviscid supersonic flow over a cone.

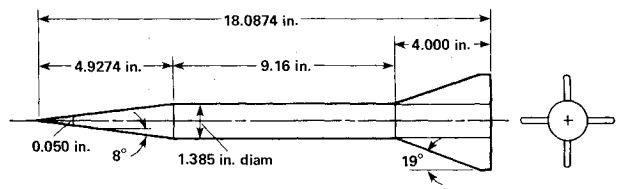

Fig. 3 Finned projectile geometry.

A peculiarity of using the space-marching technique in conjunction with the strong conservation-law form of the equations in solving conical flow problems is that $\Delta\tilde{Q}$ does not approach zero as the solution converges. Instead, $\Delta\tilde{Q}$ approaches an asymptotic value. It can be shown that $\Delta\tilde{Q}$ varies as a quadratic function of the marching distance x for a Cartesian coordinate system (x, y, z) and varies linearly with x for a cylindrical coordinate system (for conical-flow problems). Since the integration scheme used is first-order accurate in the marching direction, it is important to use cylindrical coordinates in order to obtain accurate solutions with the conical step-back procedure.

With the use of cylindrical coordinates, it can be shown, in the asymptotic limit, that the factorization error is zero for the axisymmetric case. Hence, to test the implicit boundary conditions further (for cases with nonzero factorization error), another example case was solved. It consisted of $M_\infty=3$ inviscid flow past a 15-deg cone at 10-deg incidence. Figure 2 shows iterations to convergence vs ν for this case. An acceleration factor of 26 was obtained for $\nu=23.3$ (compared with $\nu=0.7$). Unlike the $\alpha=0$-deg case, the error increased with

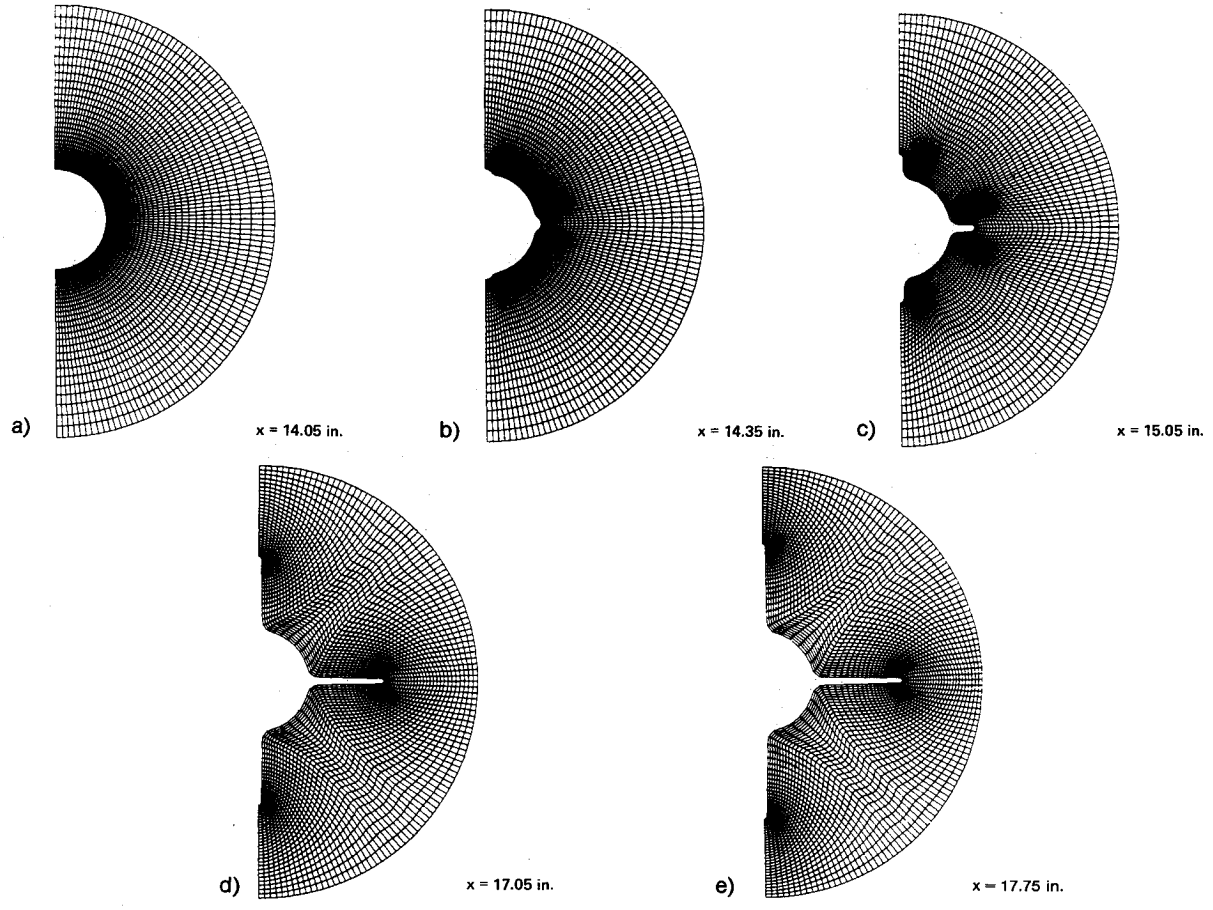

Fig. 4 Typical computational meshes in the region of the fin.

increasing ν. This is because $\Delta\tilde{Q}$ is not zero at convergence; hence, the factorization error is also nonzero. This problem will not occur for time-dependent calculations since the Jacobian of the transformation, and, hence, $\tilde{Q}$, approach asymptotic limits at convergence. The solution process became unstable for values of ν greater than 30. However, in order to limit the error in the solution, it was found necessary to limit ν to values less than 12. At a Courant number of 11.8 the acceleration factor is about 18 when compared with the convergence rate at $\nu = 0.7$, and the error in the surface density on the windward side is 1.1%.

Finned-Projectile Calculation

To substantiate the accuracy and stability of the shock-fitting option in the marching mode, the viscous hypersonic flow over a generic maneuvering re-entry vehicle was calculated. The results of this validation study can be found in Ref. 5. With the new capabilities and modifications fully tested, the PNS code was used to determine the viscous supersonic flow over a complex configuration. The configuration geometry consisted of a thick-finned projectile (Fig. 3). The freestream conditions were $M_\infty = 4$, a turbulent boundary layer with $Re/L = 10^6$/in., $T_\infty = 100°$R, $T_{\text{wall}} = 540°$R, and $\alpha = 0$ and 2 deg. Forty-five grid points were stretched in the radial direction, and 117 grid points were distributed in the circumferential direction. The starting solution at $x = 2.0$ in. was generated with the PNS code using the conical step-back procedure described earlier. The conical starting solution was then marched over the cone-cylinder portion of the projectile to $x = 13.55$ in. (which is just in front of the fins).

The grids used to calculate the flow over the finned portion of the projectile were generated using an elliptic grid generator similar to the one developed in Ref. 8. This procedure furnishes both spacing and angular control of the grid lines as they approach the boundaries of the domain such as the body and the shock. Figures 4a-e show representative grids at various streamwise x locations. The η = const grid lines intersect the body orthogonally. This is important for the accurate implementation of the viscous surface boundary conditions. The solution at $x = 13.55$ in. was then marched to the end of the projectile, using the type of grids shown in Figs. 4a-e.

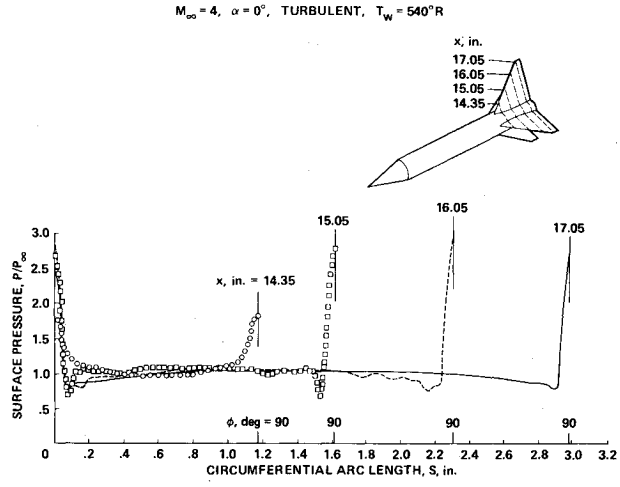

Fig. 5 Circumferential surface-pressure distributions on the finned part of the projectile.

Figures 5-8 show the results obtained for $\alpha = 0$ deg. Figure 5 shows the circumferential pressure distribution at various x stations. Because of symmetry only one quadrant is shown in the figure. Each curve represents the variation of the surface pressure as a function of the circumferential arc length. As the fins start to protrude into the flowfields, the flow is compressed and fin shocks form. The compressing of the flow

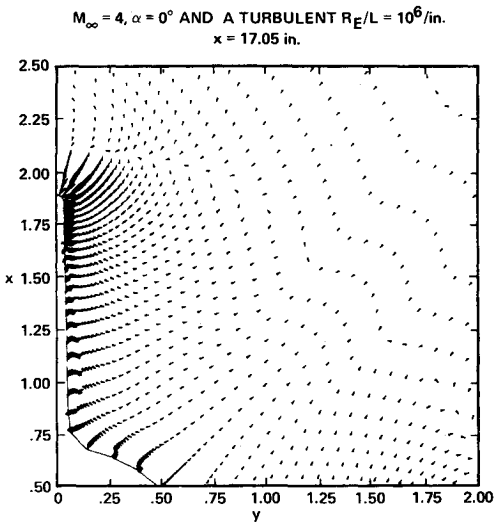

Fig. 6 Velocity vectors in the cross-flow plane at an $x = 17.05$ in. for $M_\infty = 4$, $\alpha = 0$ deg, and a turbulent $Re/L = 10^6/\text{in}$.

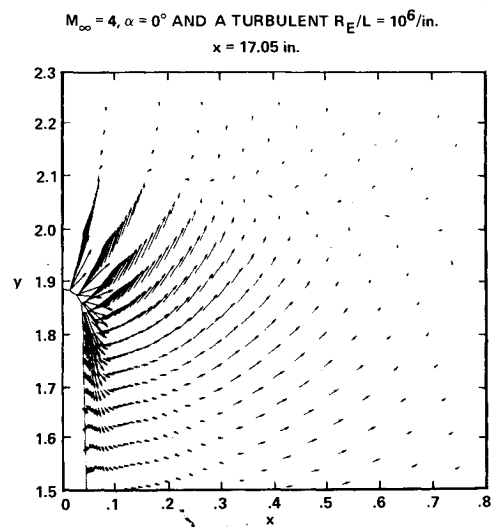

Fig. 7 Velocity vectors in the cross-flow plane at an $x = 17.05$ in. for $M_\infty = 4$, $\alpha = 0$ deg, and a turbulent $Re/L = 10^6/\text{in}$.

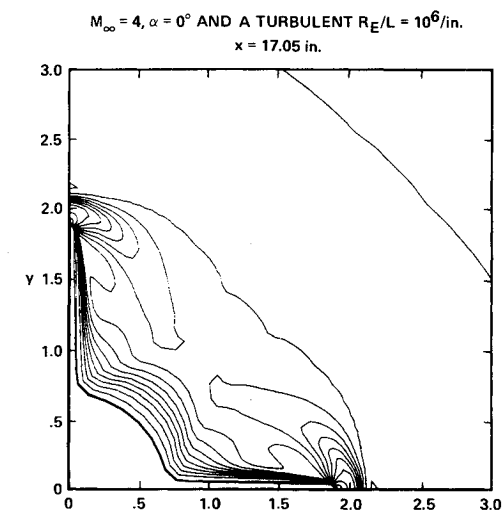

Fig. 8 Density contours in the cross-flow plane at an $x = 17.05$ in. for $M_\infty = 4$, $\alpha = 0$ deg, and a turbulent $Re/L = 10^6/\text{in}$.

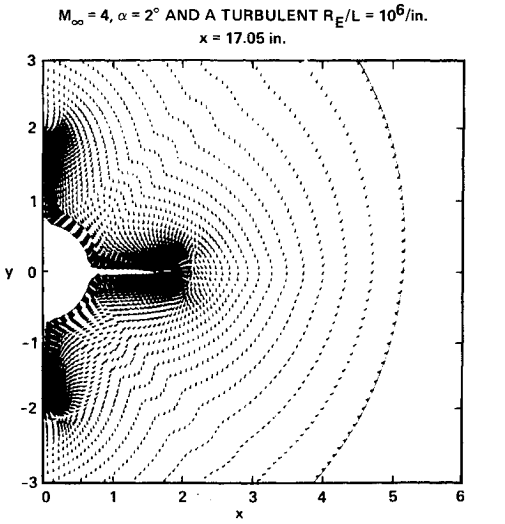

Fig. 9 Velocity vectors in the cross-flow plane at an $x = 17.05$ in. for $M_\infty = 4$, $\alpha = 2$ deg, and a turbulent $Re/L = 10^6/\text{in}$.

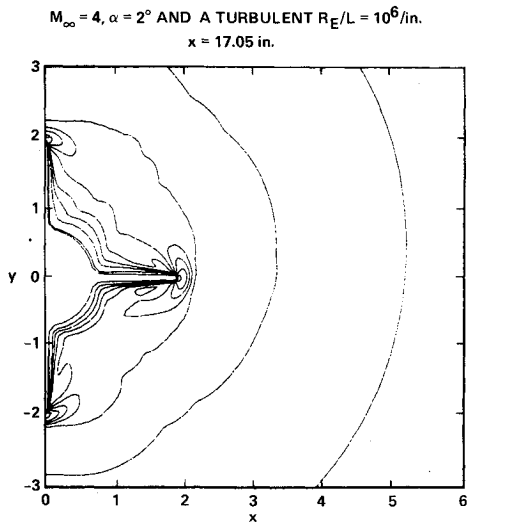

Fig. 10 Density contours in the cross-flow plane at an $x = 17.05$ in. for $M_\infty = 4$, $\alpha = 2$ deg, and a turbulent $Re/L = 10^6/\text{in}$.

caused by the fins is seen in Fig. 5 as high-pressure spikes. A strong cross-flow separation at $x = 17.05$ in. is evident in Figs. 6 and 7, which are cross-flow velocity vector plots. The separation occurs all the way from the 45-deg symmetry line to a point close to the tip of the fin. In these figures, the fin shock can also be seen as a sharp transition in the velocity direction just above the fin. Figure 8 shows the density contours at $x = 17.05$ in. The highly clustered, constant-density contours just above the fin represent the fin shock.

Figures 9 and 10 show results for the finned portion of the projectile for an angle of attack of 2 deg. Figure 9 is a cross-flow velocity vector plot at $x = 17.05$ in. The flow is no longer symmetric about the central fin, as it was for the $\alpha = 0$-deg case. The fin shocks caused by the lower and central fins can be seen in this figure but the shock caused by the upper fin is not easily observable because it is much weaker than the other two shocks. The cross-flow separation region is much larger for the $\alpha = 2$-deg case than for the $\alpha = 0$-deg case. Figure 10 shows the density contours at $x = 17.05$ in. It can be seen clearly from this figure that the shock caused by the upper fin is weaker than the shocks caused by the other fins.

The implicit shock procedure facilitated the finned projectile calculation in two ways. First, the conical starting solution used for the calculation was generated in 150 iter-

ations instead of 2400 iterations (the number of steps required for convergence with the explicit shock-fitting routine). Second, the marching step size did not have to be monitored constantly. With the explicit shock procedure, the marching step size has to be checked at every step and reduced whenever the CFL number at the shock approaches 0.7. These abrupt changes in step size usually have a detrimental effect on the accuracy of the calculation. While accuracy considerations usually require the use of small marching steps (resulting in shock CFL numbers between 0.1 and 2.0 and, consequently, not making maximum use of the implicit shock procedure), approximate initial solutions in a design environment can be obtained very rapidly by taking large step sizes with the help of implicit boundary procedures.

Conclusions

A new implicit boundary procedure for the inviscid equations of motion has been developed. The procedure uses the theory of characteristics to update boundary points, is spatially second-order accurate, and is simple to incorporate into existing codes. The boundary information is brought in so that it is not affected by the approximate factorization. This results in more accurate calculations. The boundary scheme has been incorporated into an existing PNS code at the body and the shock boundaries, thus giving the code a totally implicit inviscid capability. The results presented in this paper have been obtained with the Beam-Warming scheme. The implicit boundary procedure, however, can be used with other implicit integration schemes like the split-flux scheme of Steger and Warming[9] with minor modifications. The amount of computer time required to incorporate the implicit boundary conditions is a small fraction of the time required for one integration step (less than 5%).

Results demonstrating a significant increase in convergence rates have been obtained for conical flow problems. For the first time, the flow over a finned projectile has been calculated using the PNS code with the new boundary conditions. The implicit boundary procedure has been found to be stable and accurate in the marching mode.

References

[1]Chakravarthy, S.R., "Euler Equations—Implicit Schemes and Implicit Boundary Conditions," AIAA Paper 82-0228, Jan. 1982.

[2]Chaussee, D.S., Patterson, J.L., Kutler, P., Pulliam, T.H., and Steger, J.L., "A Numerical Simulation of Hypersonic Viscous Flow over Arbitrary Geometries at High Angle of Attack," AIAA Paper 81-0050, Jan. 1981.

[3]Chakravarthy, S.R., "The Split-Coefficient Matrix Method for Hyperbolic Systems of Gas Dynamic Equations," Ph.D. Thesis, Dept. of Aerospace Engineering, Iowa State Univ., Ames, Iowa, 1979.

[4]Beam, R.M. and Warming, R.F., "An Implicit Factored Scheme for the Compressible Navier-Stokes Equations," *Proceedings of the AIAA 3rd Computational Fluid Dynamics Conference*, Albuquerque, N. Mex., June 1977.

[5]Rai, M.M. and Chaussee, D.S., "New Implicit Boundary Procedures: Theory and Applications," AIAA Paper 83-0123, Jan. 1983.

[6]Schiff, L.B. and Steger, J.L., "Numerical Simulation of Steady Supersonic Viscous Flow," AIAA Paper 79-0130, Jan. 1979.

[7]Kutler, P., "Application of Selected Finite Difference Techniques to the Solution of Conical Flow Problems," Ph.D. Thesis, Dept. of Aerospace Engineering, Iowa State Univ., Ames, Iowa.

[8]Steger, J.L. and Sorenson, R.L., "Automatic Mesh-Point Clustering near a Boundary in Grid Generation with Elliptic Partial Differential Equations," *Journal of Computational Physics*, Vol. 33, No. 3, Dec. 1979, pp. 405-410.

[9]Steger, J.L. and Warming, R.F., "Flux Vector Splitting of the Inviscid Gas Dynamics Equations with Application to Finite Difference Methods," *Journal of Computational Physics*, Vol. 40, No. 2, April 1981, pp. 263-293.